Supplementary Information

Multifunctional sandwich-structured double-carbon-layer modified SnS nanotubes with high capacity and stability for Li-ion batteries

Jia Luo[a, b], Huaiyu Li[a, b], Guo Yu[a, b], Wenyuan Xu[a, b], Hong Yin[a, b, *], Zhaohui Hou[a, b, **]

[a]School of Chemistry and Chemical Engineering, Hunan Institute of Science and Technology, Yueyang, 414006, China

[b]Key Laboratory of Hunan Province for Advanced Carbon-based Functional Materials, Hunan Institute of Science and Technology, Yueyang 414006, China

*Corresponding Author

E-mail: 2017507027@hust.edu.cn (H. Yin).

*, *Corresponding Author

E-mail: zhaohuihou@126.com (Z. Hou).

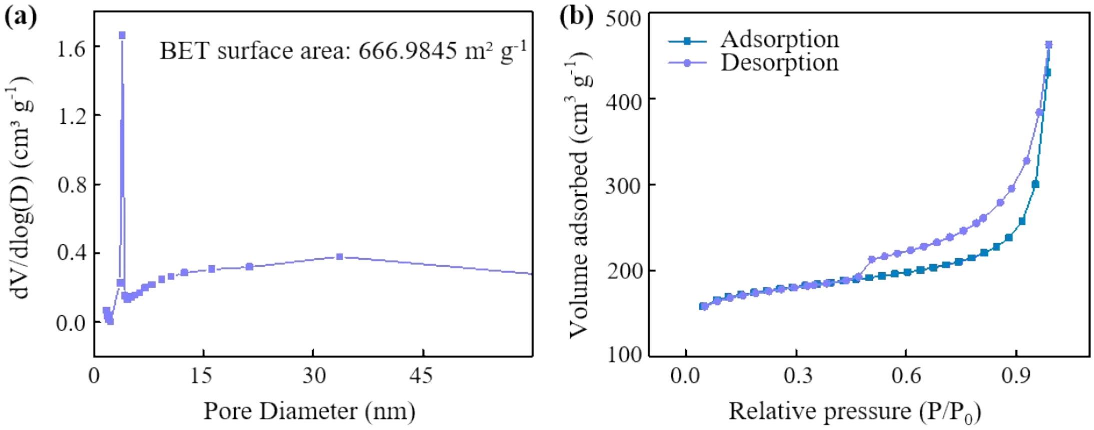

Figure S1. Pore size distribution (a) and N_2 adsorption-desorption isotherms (b) of the as-prepared N-DCSNs.

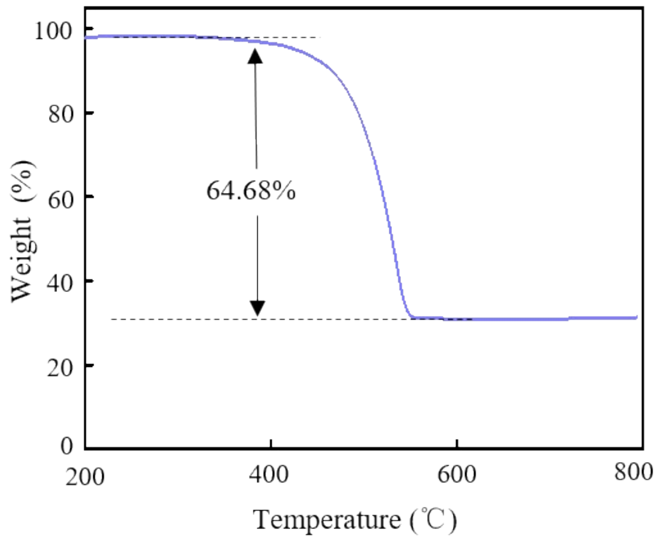

Figure S2. TG analysis of N-DCSNs sample at temperatures ranging from 200 to 800 ℃ in air.

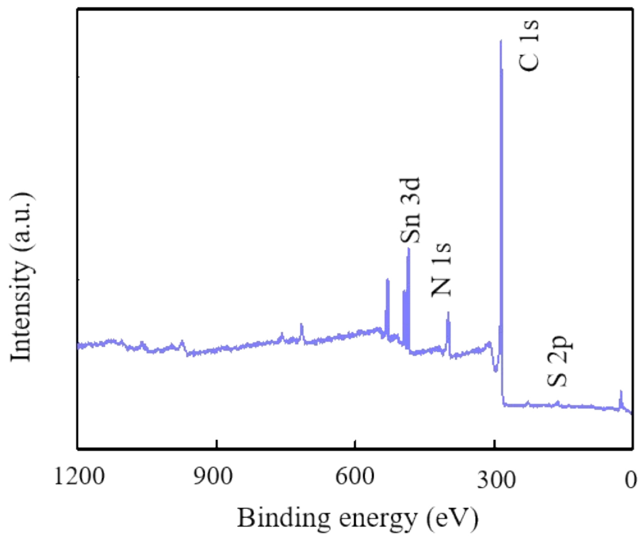

Figure S3. XPS spectra of N-DCSNs for all elements.

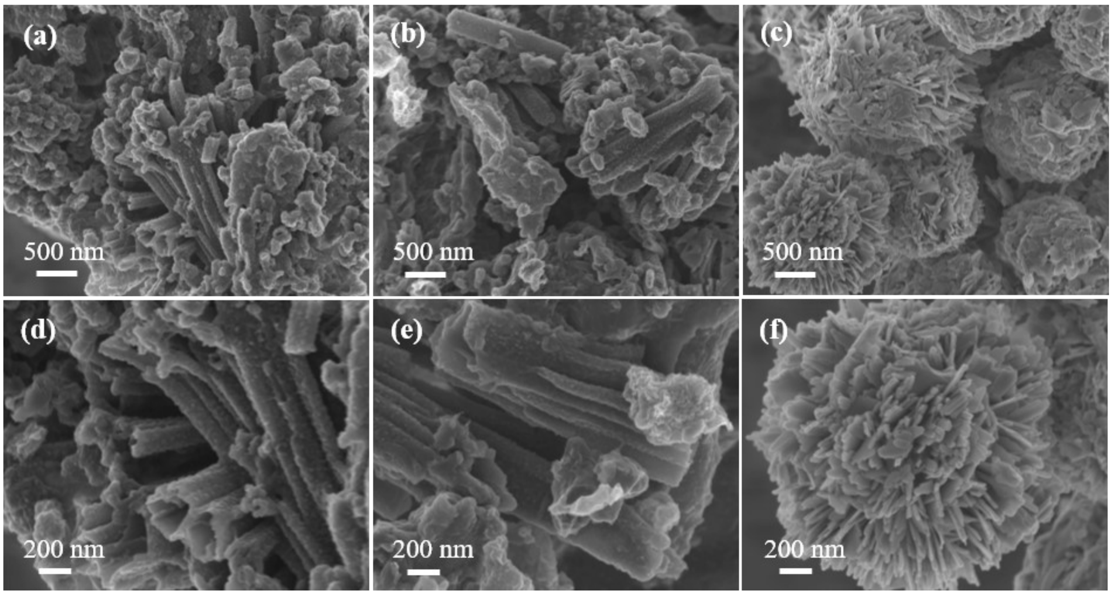

Figure S4. SEM images of the N-DCSNs (a, d), the CN/SnS composites (b, e) and the bare SnS (c, f).

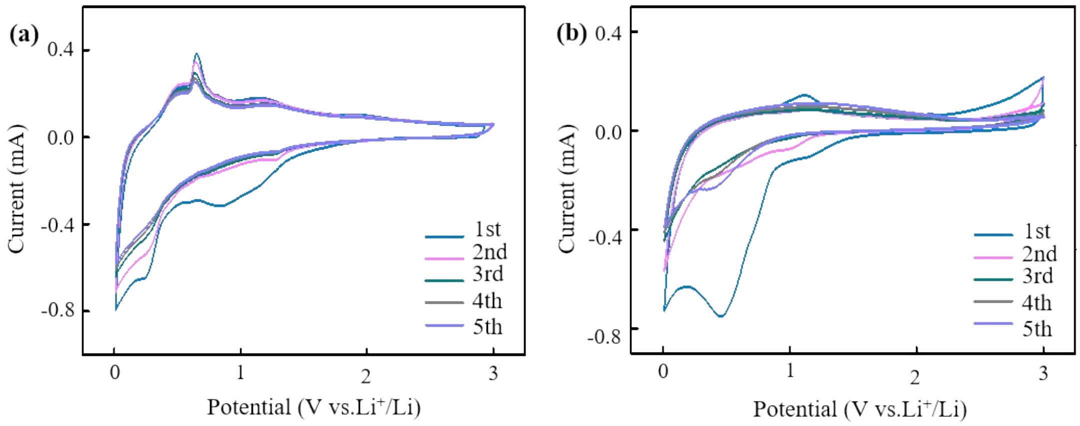

Figure S5. Cyclic voltammetry curves of CN/SnS (a) and bare SnS (b) between 0.01 and 3.0 V with a scan rate of 0.5 mV s^{-1}.

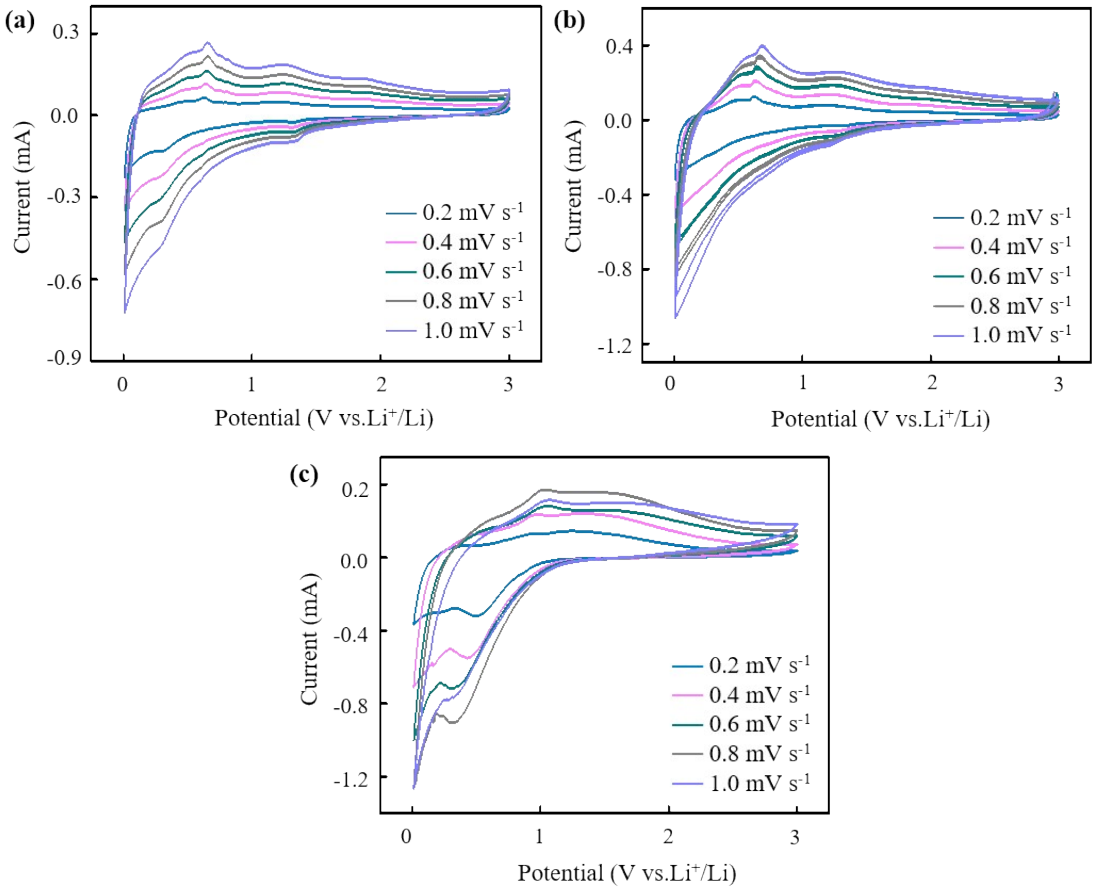

Figure S6. Cyclic voltammetry curves of N-DCSNs (a), CN/SnS (b) and bare SnS (c) between 0.01 and 3.0 V with scan rate of 0.2, 0.4, 0.6, 0.8, and 1.0 mV s^{-1}, respectively.

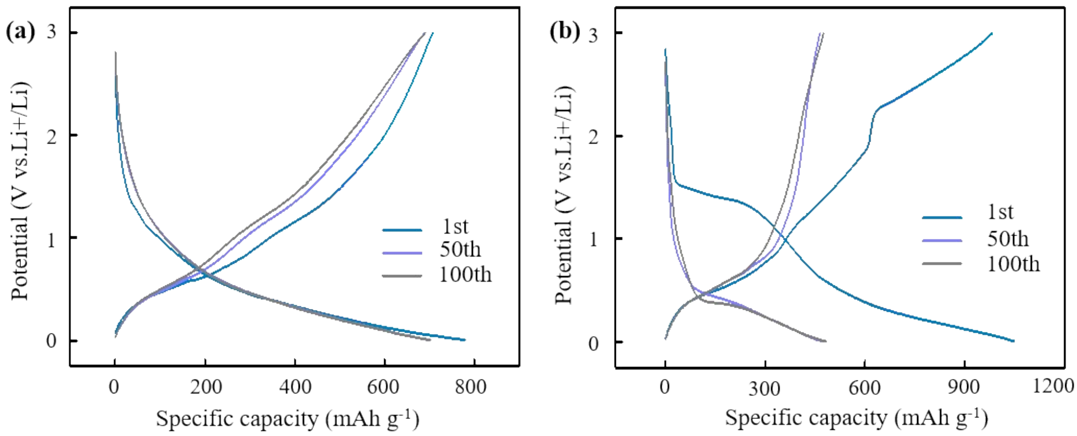

Figure S7. Discharge-charge voltage profiles of CN/SnS (a) and bare SnS (b) at a current density of 0.2 A g^{-1}, respectively.

Table S1. Electrochemical performance of SnS-based anode materials for LIBs.

Samples	Specific capacity (mAh g^{-1})	Cycles	Current density (A g^{-1})	Ref.
SnS/N-G	1120	130	0.1	[1]
SnS@C HSs	532	100	0.1	[2]
SnS/N-C particles	535	300	1.0	[3]
SnS/C nanofibers	648	500	0.2	[4]
3D porous SnS/C	607	200	1.0	[5]
SnS nanoparticles	410	50	0.1	[6]
SnS nanoflowers	600	30	0.05	[7]
SnS/C-CP	696	200	0.5	[8]
SnS NS/RGO	560	100	0.1	[9]
SnS-ZnS@C	302	500	0.5	[10]
3D SnS flowers	360	50	0.8	[11]
SnS-PNA	900	50	0.3	[12]
C@SnS/SnO_2@CNFs	917	200	0.2	[13]
N-DCSNs	**911.5**	**270**	**0.2**	**This work**
	511.3	**1000**	**1.0**	

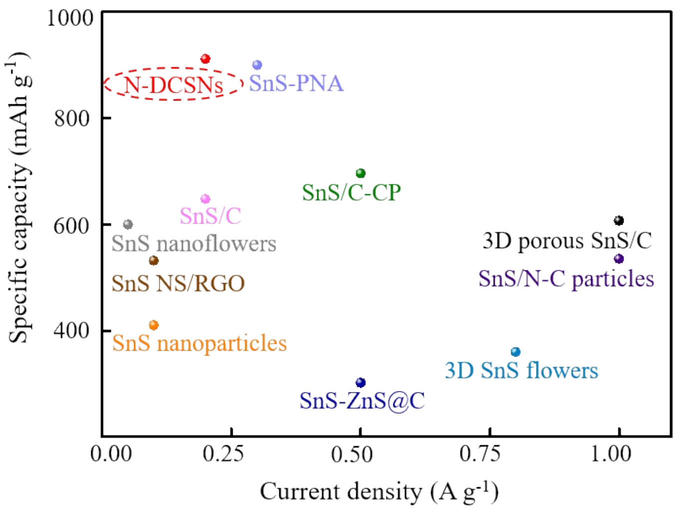

Figure S8. Electrochemical performance of SnS-based anode materials for LIBs.

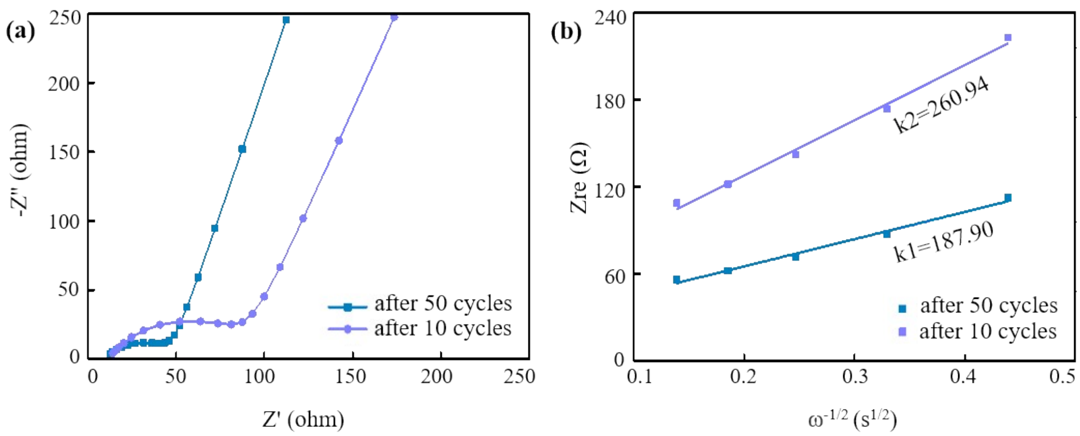

Figure S9. (a) Nyquist plots of N-DCSNs electrodes measured in the frequency region of 10^5-10^{-2} Hz after 10 and 50 cycles. (b) The real part of the complex impedance versus $\omega^{-1/2}$ at open circuit voltage for N-DCSNs electrodes after 10 and 50 cycles.

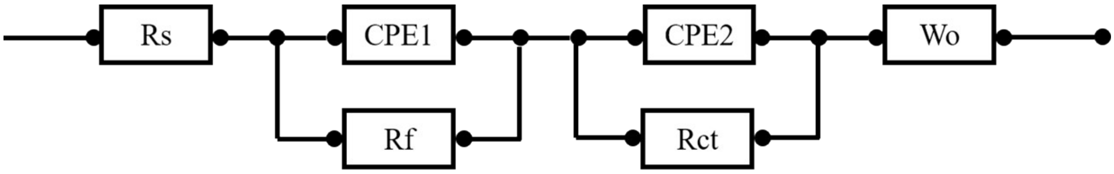

Figure S10. Equivalent circuit model for the simulation of the Nyquist plots.

R_s is the electrolyte resistance, R_f is surface film resistance, R_{ct} is charge transfer resistance, W_o is the Warburg impedance related to the diffusion of Li-ion into electrodes, *CPE1* and *CPE2* represent the constant phase elements.

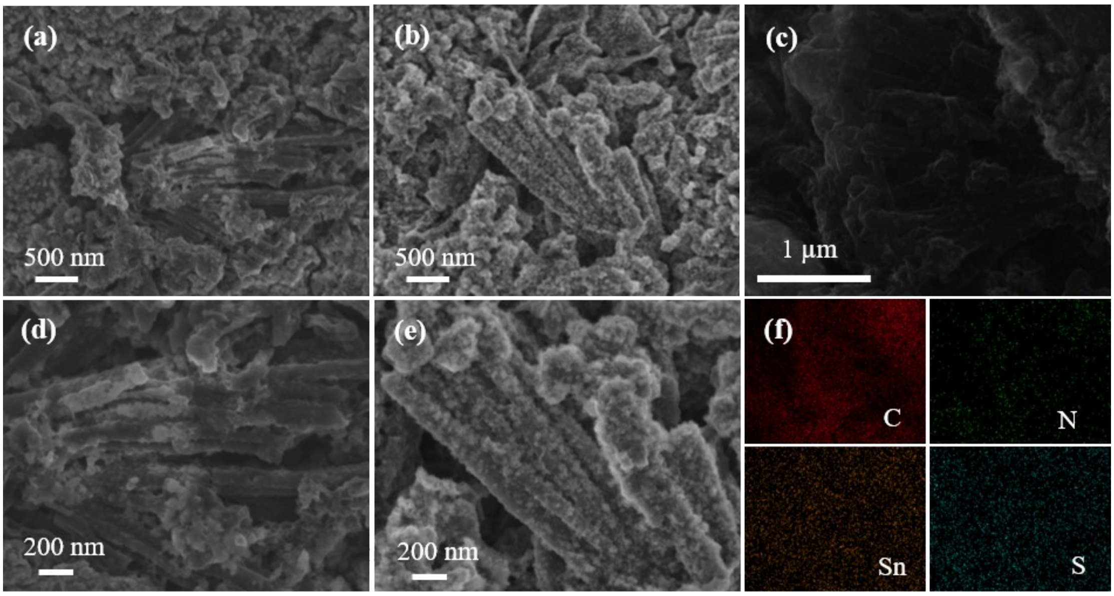

Figure S11. SEM images of N-DCSNs electrodes after 60 cycles (a, d) and 270 cycles (b, e) at 0.2 A g^{-1}. (e, f) EDS images with the corresponding element distribution images of N-DCSNs.

Table S2. Impedance parameters of N-DCSNs, CN/SnS and SnS electrodes before cycling obtained by the equivalent circuit model.

Samples	R_s (Ω)	R_f (Ω)	R_{ct} (Ω)
N-DCSNs	1.928	48.98	36.68
CN/SnS	2.905	51.2	57.19
SnS	2.104	72.06	61.77

Table S3. The linear relevant fitting result of the N-DCSNs, CN/SnS and bare SnS electrodes, respectively.

Slope	N-DCSNs	CN/SnS	SnS
Before cycle	105.57	116.08	75.99
After 50 cycles	187.90	372.11	313.28

Depiction S1. Electric conductivity & Li-ion diffusion coefficient at open circuit state:[14-17]

$$D = R^2T^2/2A^2n^4F^4C^2\sigma^2 \text{......} (1) \quad Z_{Re} = R_e + R_{ct} + \sigma\omega^{-1/2} \text{......} (2)$$

where D is the diffusion coefficient ($cm^2\ s^{-1}$), R is the gas constant (8.31 $J\ mol^{-1}\ K^{-1}$), T is the absolute temperature (298 K), A is the surface area of the anode (0.36 cm^2), n is the number of electrons transferred in the half-reaction for the redox couple, F is the Faraday constant (96485 $C\ mol^{-1}$), C is the is the molar concentration of Li-ion in N-DCSNs, R_e is the resistance between the electrolyte and electrode, R_{ct} is the charge transfer resistance, ω is frequency, and σ is the Warburg factor which corresponds to the slope of the curve shown in **Figure 5c, d**.

Depiction S2. The chemical diffusion coefficients of the electrodes in LIBs are determined by formulas 3 and 4:[18]

$$D = \frac{4}{\pi}\left(\frac{I_0 V_M}{S F z_i}\right)^2 \left[\frac{dE}{d\delta} \Big/ \frac{dE}{d\sqrt{\tau}}\right]^2 \left(\tau \ll \frac{L^2}{D}\right) \quad (3) \qquad D = \frac{4}{\pi\tau}\left(\frac{m_B V_M}{S M_B}\right)^2 \left(\frac{\Delta E_s}{\Delta E_\tau}\right)^2 \left(\tau \ll \frac{L^2}{D}\right) \quad (4)$$

The parameters required for D value can be obtained from the known conditions according to formula 4, τ is the excitation current time (s), S is the electrode area (cm^2), ΔE_s is the steady-state voltage change (V), ΔE_τ is the transient voltage change (V), V_M is the molar volume of electrode material (cm^3 mol^{-1}), m_B is the mass of the electrode material (g), and M_B is the molar mass of the electrode material (g mol^{-1}).

References:

1. Yao, L.; Nie, M.; Zhu, C.; Cai, R.; Xia, W.; Sun, L.; Xu, F., Revealing a conversion-alloying reaction mechanism behind high capacity and rate capability of SnS/N-doped graphene anode by in situ TEM. *Electrochim. Acta.* **2019,** *297*, 46-54.

2. Guo, W.; Ding, K.; Mei, S.; Li, X.; Feng, X.; Guo, S.; Fu, J.; Zhang, X.; Gao, B.; Huo, K.; Chu, P. K., Hollow spheres consisting of SnS nanosheets conformally coated with S-doped carbon for advanced lithium/sodium-ion battery anodes. *ChemElectroChem* **2020,** *7* (4), 914-921.

3. Jin, A.; Kang, N.; Um, J. H.; Ko, I. H.; Kim, M. S.; Kim, K.; Kim, S. H.; Yu, S. H.; Sung, Y. E., Sn(salen)-derived SnS nanoparticles embedded in N-doped carbon for high performance lithium-ion battery anodes. *Chem. Commun.* **2020,** *56* (58), 8095-8098.

4. Xia, J.; Liu, L.; Jamil, S.; Xie, J.; Yan, H.; Yuan, Y.; Zhang, Y.; Nie, S.; Pan, J.; Wang, X.; Cao, G., Free-standing SnS/C nanofiber anodes for ultralong cycle-life lithium-ion batteries and sodium-ion batteries. *Energy Stor. Mater.* **2019,** *17*, 1-11.

5. Zhu, C.; Kopold, P.; Li, W.; van Aken, P. A.; Maier, J.; Yu, Y., A general strategy to fabricate carbon-coated 3D porous interconnected metal sulfides: case study of SnS/C nanocomposite for high-performance lithium and sodium ion batteries. *Adv. Sci.* **2015,** *2* (12), 1500200.

6. Manukumar, K. N.; Nagaraju, G.; Kishore, B.; Madhu, C.; Munichandraiah, N., Ionic liquid-assisted hydrothermal synthesis of SnS nanoparticles: Electrode materials for lithium batteries, photoluminescence and photocatalytic activities. *J. Energy Chem.* **2018,** *27* (3), 806-812.

7. Vaughn, D. D.; Hentz, O. D.; Chen, S.; Wang, D.; Schaak, R. E., Formation of SnS nanoflowers for lithium ion batteries. *Chem. Commun.* **2012,** *48* (45), 5608-5610.

8. Zheng, J.; Luo, Y.; Xie, D.; Xiong, X.; Lin, Z.; Wang, G.; Yang, C.; Liu, M., One-pot synthesis of SnS/C nanocomposites on carbon paper as a high-performance free-standing anode for lithium ion batteries. *J. Alloys Compd.* **2019,** *779*, 67-73.

9. Li, S.; Zheng, J.; Zuo, S.; Wu, Z.; Yan, P.; Pan, F., 2D hybrid anode based on SnS

nanosheet bonded with graphene to enhance electrochemical performance for lithium-ion batteries. *RSC Adv.* **2015,** *5* (58), 46941-46946.

10. Zhang, Y.; Wang, P.; Yin, Y.; Zhang, X.; Fan, L.; Zhang, N.; Sun, K., Heterostructured SnS-ZnS@C hollow nanoboxes embedded in graphene for high performance lithium and sodium ion batteries. *Chem. Eng. J.* **2019,** *356*, 1042-1051.

11. Cho, E.; Song, K.; Park, M. H.; Nam, K. W.; Kang, Y. M., SnS 3D flowers with superb kinetic properties for anodic use in next-generation sodium rechargeable batteries. *Small* **2016,** *12* (18), 2510-2517.

12. Choi, J.; Kim, N. R.; Lim, K.; Ku, K.; Yoon, H. J.; Kang, J. G.; Kang, K.; Braun, P. V.; Jin, H. J.; Yun, Y. S., Tin Sulfide-Based Nanohybrid for High-Performance Anode of Sodium-Ion Batteries. *Small* **2017,** *13* (30), 1700767.

13. Lian, Q.; Zhou, G.; Zeng, X.; Wu, C.; Wei, Y.; Cui, C.; Wei, W.; Chen, L.; Li, C., Carbon coated SnS/SnO_2 heterostructures wrapping on CNFs as an improved-performance anode for Li-ion batteries: lithiation-induced structural optimization upon cycling. *ACS Appl. Mater. Interfaces* **2016,** *8* (44), 30256-30263.

14. Yin, H.; Shen, W.; Qu, H.-Q.; Li, C.; Zhu, M.-Q., Boosted charge transfer and Na-ion diffusion in cooling-fins-like Sb_2Te-Te nano-heterostructure for long cycle life and high rate capability anode. *Nano Energy* **2020,** *70*, 104468.

15. Jae-Min; Jeong, Ultrathin sandwich-like MoS_2@N-doped carbon nanosheets for anodes of lithium ion batteries. *Nanoscale* **2015,** *1* (7), 324-329.

16. Ai, W.; Huang, Z.; Wu, L.; Du, Z.; Zou, C.; He, Z.; Shahbazian-Yassar, R.; Huang, W.; Yu, T., High-rate, long cycle-life Li-ion battery anodes enabled by ultrasmall tin-based nanoparticles encapsulation. *Energy Stor. Mater.* **2018,** *14*, 169-178.

17. Yin, H.; Yu, X.-X.; Zhao, H.; Li, C.; Zhu, M.-Q., Towards high-performance cathode materials for lithium-ion batteries: Al_2O_3-coated $LiNi_{0.8}Co_{0.15}Zn_{0.05}O_2$. *J. Solid. State. Electr.* **2018,** *22* (8), 2395-2403.

18. Zhu, S.; Yin, H.; Wang, Y.; Hui, K. S.; Wu, X.-L.; Mai, W.; Hong, X.; Chen, F.; Hui, K. N., Heteroatomic interface engineering of MOF-derived metal-embedded P and N-codoped Zn node porous polyhedral carbon with enhanced sodium-ion storage. *ACS Appl. Energy Mater.* **2020,** *3* (9), 8892-8902.